TECHNICAL UNIVERSITY OF CLUJ-NAPOCA

ACTA TECHNICA NAPOCENSIS

Series: Applied Mathematics, Mechanics, and Engineering
Vol. 67, Issue Special IV, August, 2024

CFD ESTIMATION OF PRESSURE DROP COEFFICIENTS FOR SQUEEZE FILM DAMPERS WITH PISTON RING GROOVES

Emanuele GIAMPAOLO, Mihai ARGHIR, Hugo FESTJENS

Abstract: *Squeeze film dampers (SFDs) are used in aeronautical engines to add damping to flexible rotors guided by ball and roller bearings. Theoretical analysis of SFDs faces challenges due to high-speed operation and grooves geometry which contradicts the thin film hypothesis on which the theory of lubrication is built on. Reynolds' equation yields acceptable predictions only for simple SFDs at low speeds, inadequate for modern ensemble dynamic analyses of aircraft engines. Computational Fluid Dynamics (CFD) offers accurate but computationally intensive solutions. An alternative, the bulk flow (BF) system of equations, is capable of handling convective inertia-dominated regimes (prohibitive with a Reynolds-like approach), with significantly lower computational costs. Feeding and piston ring grooves are taken into account in the BF model by using local pressure drop or recovery coefficients. Therefore, the BF approach relies on the determination of these externally defined coefficients, challenging to predict experimentally. CFD predictions are then a viable alternative to estimate these coefficients. In this work, we show how local information about pressures and velocities obtained from CFD can be used to improve the BF models.*
Key words: *Squeeze Film Dampers, Piston Rings, Piston Ring Clearances, Piston Ring Grooves, CFD, Bulk-flow.*

1. INTRODUCTION

Squeeze film dampers (SFDs) are components of rotating machinery. They play a central role in limiting the rotor response to residual imbalance and grant rotor-dynamic stability [1]. They consist of a thin film of oil positioned in between the outer ring of a rolling bearing and the damper housing. An anti-rotation pin or a squirrel cage are used to prevent the rotation of the outer race of the bearing (Fig. 1). Due to the imbalance of the rotor, the bearing outer ring undergoes a precession movement that squeezes the oil. The forces generated by the SFD are only due to this squeezing effect. The oil is supplied to the film via feeding orifices that can discharge it directly into the film, or into a feeding groove. O-rings, piston rings (PRs) and end plates are commonly used as end seals for SFDs [2]. They prevent excessive oil outflow and enhance the performances of the damper. To limit the temperature rise inside the thin film, some of the heat generated by friction inside the damper has to be evacuated. Slits are cut into the PRs, allowing some oil to exit the SFD, thus evacuating part of the heat. This is an important aspect in SFDs since an excessive temperature rise would make the viscosity diminish, therefore impacting the damper performances. Although accurate, CFD of SFDs demands important computational resources. In classical lubrication problems, the Reynolds equation is the most common alternative to the complete Navier-Stokes equations. However, the operating conditions of SFDs often lead to inertia-dominated flows where the classical Reynolds formulation cannot be used.

The bulk-flow approach is considered as an alternative to CFD, that is less resources intensive, and can be applied to inertia dominated flows. When developing a simplified model for SFDs, CFD results can be used as a powerful tool to validate and tune coefficients appearing in the simplified formulation. The present work shows how this possibility has been exploited to treat the problem of correctly considering piston ring clearances.

When PRs are installed in their grooves, two clearances characterize the space between the seal and the rotor of the SFD. Following the

nomenclature introduced by Lee [3], it is possible to distinguish a radial clearance C_r of length L_w and an axial clearance C_a whose length depend on the height of the PR, L_h, and on the local clearance C (Fig. 2).

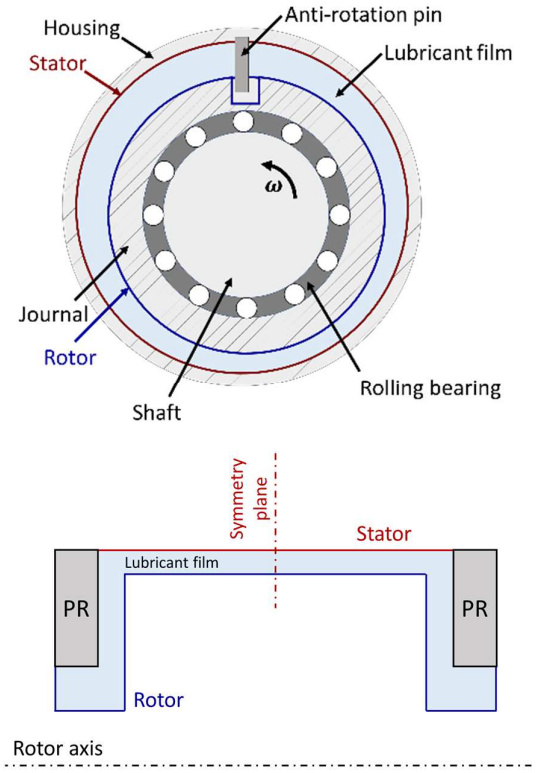

Fig. 1. Typical architecture of a SFD with anti-rotation pin (top) and axial section of a SFD with PRs (bottom).

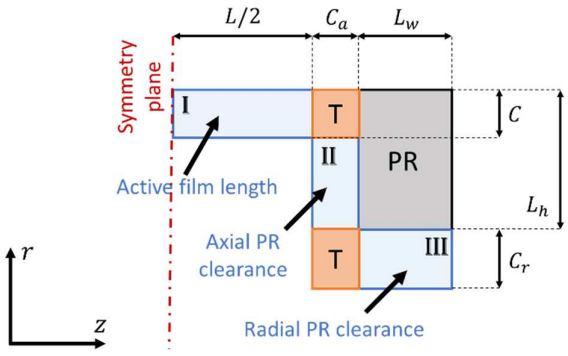

Fig. 2. PR grooves dimensions.

The geometry of a SFD can be divided in different thin film regions, corresponding to the active length of the SFD (I), the axial PR clearance (II) and the radial PR clearance (III). The thin film regions are separated by transition zones (T), where the direction of the flow changes abruptly (Fig. 2). CFD calculations on a simplified SFD were used to characterize the pressure drop occurring in the transition zones because of the abrupt flow deviation. Using insights from the CFD analysis, a model was developed and adjusted to consider the contributions of transition regions within a BF model.

2. THEORETICAL APPROACH

2.1 The bulk-flow equations

The bulk-flow equations are suitable for inertia dominated thin film flows, i.e., $Re^* = \frac{\rho\omega C^2}{\mu} > 1$. In aeronautical applications of SFDs, the typical operating conditions are in this domain. For a thin film aligned with the axial coordinate, the BF equations for the unwrapped SFD write:

$$\begin{cases} \dfrac{\partial(\rho H)}{\partial t} + \dfrac{\partial(\rho U H)}{\partial x} + \dfrac{\partial(\rho W H)}{\partial z} = 0, \\ \dfrac{\partial(\rho U H)}{\partial t} + \dfrac{\partial(\rho U^2 H)}{\partial x} + \dfrac{\partial(\rho U W H)}{\partial z} = \\ \qquad -H\dfrac{\partial P}{\partial x} - \tau_{Sx} - \tau_{Rx}, \\ \dfrac{\partial(\rho W H)}{\partial t} + \dfrac{\partial(\rho W U H)}{\partial x} + \dfrac{\partial(\rho W^2 H)}{\partial z} = \\ \qquad -H\dfrac{\partial P}{\partial z} - \tau_{Sz} - \tau_{Rz}. \end{cases} \quad (1)$$

Similar equations can be written for a thin film aligned with the r direction (as in the axial PR clearances). The solution of system (1) passes through the integration of the BF equations over time and a control volume. The integrated equations are then discretized and solved using, for example, the SIMPLE (Semi-Implicit Method for Pressure-Linked Equations) algorithm [4], as done in [5] for a SFD without PR grooves. When PR grooves are considered, transition regions appear in the domain. In these regions, the BF equations (1) do not apply since the thin film hypothesis are not verified. A specific treatment of the problem is needed in this case. In the following, the strategy adopted for considering the contribution of the transition regions is detailed.

2.2 Model for the transition regions

Fig. 3 shows the discretization near the transition region in between the active film length of the SFD and the right axial PR clearance. The cells are organized following a local coordinate s, aligned with z in the active length of the SFD and in the radial PR clearances, and with r in the axial PR clearances.

The transition region reduces to a discontinuity between the cells P and E (east), respectively on the left and on the right of the transition region. The cell P has its east limit in contact with the transition region, while the cell E has its west limit in contact with it. The passage of the flow in the transition regions is modelled by imposing the mass conservation and a Bernoulli-like relation to describe the energy losses. For a centered SFD, the mass conservation equation and the generalized Bernoulli equation between the cells P and E write:

$$\rho_P^e W_P^e H_P^e dx = \rho_E^w W_E^w H_E^w dx, \qquad (2a)$$

$$P_P^e + \xi_P^e \frac{\rho_e (W_P^e)^2}{2} = P_E^w + \xi_E^w \frac{\rho_e (W_E^w)^2}{2}. \qquad (2b)$$

The value of the pressure drop coefficients, ξ_P^e, ξ_E^w depend on the direction of the flow, i.e.:

$$\xi_P^e = (1+\xi) \cdot \frac{1 - sign(W)}{2}, \qquad (3a)$$

$$\xi_E^w = (1+\xi) \cdot \frac{1 + sign(W)}{2}. \qquad (3b)$$

It is assumed that neither the mass conservation nor the Bernoulli equations are influenced by the circumferential flow. This is true for a centered SFD and has been extended for simplicity to the case of eccentric rotors.

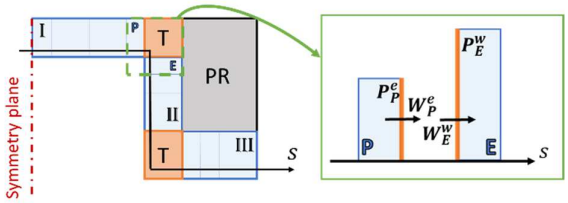

Fig. 3. Discretization near a transition region.

P_P^e and P_E^w are calculated by solving equations $(2a, b)$ at each iteration of the SIMPLE algorithm. This approach is similar to the one used in [6] for dealing with the thin film height discontinuity introduced by feeding grooves.

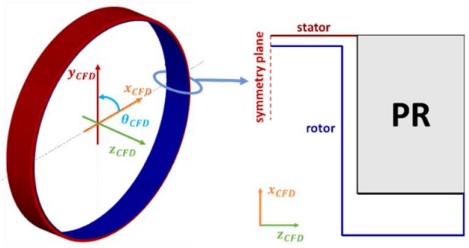

Fig. 4. CFD calculation domain, 3D and axial section ($\theta_{CFD} = 0°$) visualizations.

In general, the two transition zones are characterized by a different pressure drop. Two different loss coefficients ξ are therefore needed to characterize the two transition regions: ξ_1 is the coefficient that is used to describe the pressure drop at the transition region in between the active film length and the axial PR clearance. ξ_2 is the coefficient used to model the pressure drop occurring in the transition region in between the PR clearances. CFD calculations on a simplified SFD geometry were realized to characterize the pressure drop in these two transition regions.

2.3 Geometry used in the CFD calculations

Fig. 4 shows a representation of the computational domain. The simplified SFD used for CFD calculations has no inlets nor outlets. Only half of the SFD was simulated using a symmetry boundary condition at the axial mid-length. PRs ensure the sealing of the SFD. The geometry is characterized by the following normalized lengths: $R_r/C \cong 400$, $L/C \cong 200$, $C_a/C \cong 1$, $C_r/C \cong 5$, $L_h/C = L_w/C \cong 10$, $C_a/L_h \cong 0.1$ and $C_r/L_w \cong 0.5$. When solving the Navier-Stokes equations in a rotating reference frame following the whirl of the eccentric rotor, a quasi-steady solution is obtained. This approach for SFDs has been validated by Lee [3].

The oil used in the simulations is the Hydro Jet II at 120°C, characterized by $\rho = 938\, kg/m^3$ and $\mu = 3.474 \cdot 10^{-3}\, Pa\, s$. The relative eccentricity was fixed at $\varepsilon = 0.3$ in the x_{CFD} direction (corresponding to $\theta_{CFD} = 0$) and two reduced Reynolds numbers where considered: $Re^* = 1$ and $Re^* = 5$. Reynolds numbers smaller than 1 were avoided because the BF model is adapted only for inertia-dominated flows, i.e., $Re^* \geq 1$.

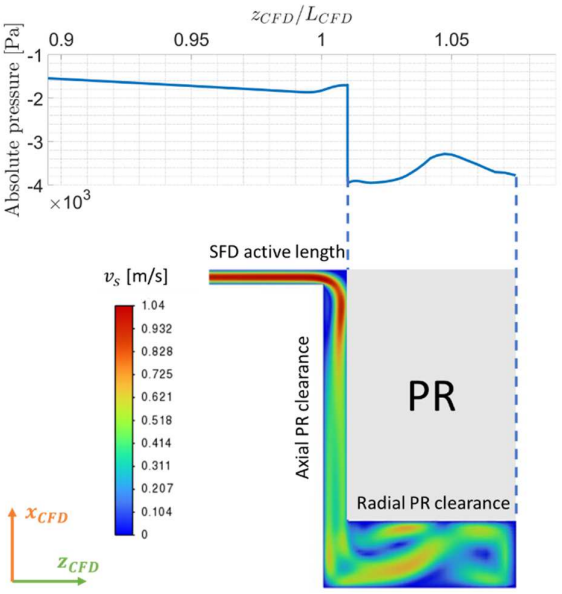

Fig. 5. Velocity and pressure inside the PR clearances.

3. RESULTS

To obtain an estimation of the coefficients ξ_1 and ξ_2, CFD results were compared to BF results obtained for different values of the coefficients. Preliminarily, an analysis of the CFD results alone was made to obtain some insight in the physics inside the transition regions. Fig. 5 shows the velocity $v_s = \sqrt{v_{x_{CFD}}^2 + v_{z_{CFD}}^2}$ and pressure profiles inside the PR grooves for the section at $\theta_{CFD} = 0°$. When the fluid enters the axial PR clearance, a clear pressure drop is observed.

On the contrary, no clear abrupt variations of the pressure are present when the fluid enters the radial PR clearance. This is explained by the fact that the transition zone between the active land of the SFD and the axial PR clearance is characterized by higher velocities.

Following these observations, $\xi_2 = -1$, meaning that $P_P^e = P_E^w$. For the other transition region, ξ has to be chosen to mimic the pressure drop observed in the CFD results, i.e. $\xi_1 > 0$. CFD and BF results obtained for different values of ξ_1 were compared to find the optimal value for this loss coefficient.

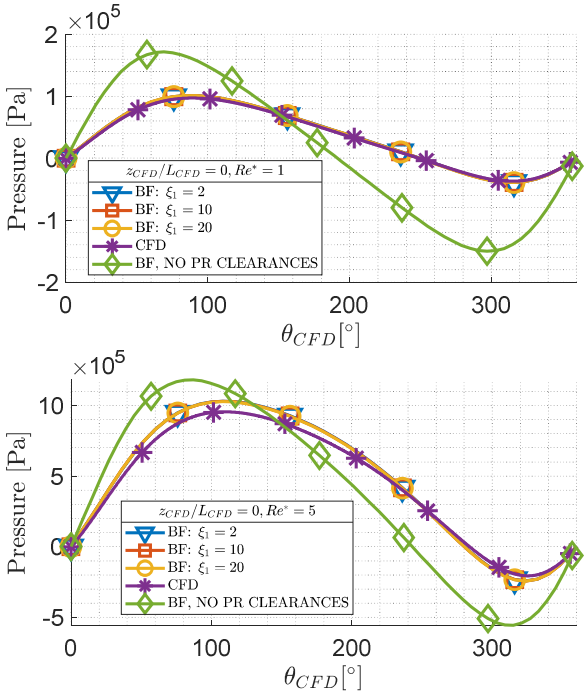

Fig. 6. Circumferential pressure variation $Re^* = 1$ (top) and $Re^* = 5$ (bottom).

Fig. 6 shows the circumferential pressure variation at the axial mid-length of the SFD ($z_{CFD} = 0$), for both $Re^* = 1$ (top) and $Re^* = 5$ (bottom). Both the CFD and BF calculations are performed considering an incompressible fluid and a closed SFD.

When no external pressure boundary conditions are imposed on the calculation, the pressure results are known up to a constant. To fix this constant and compare BF and CFD pressure solutions, the pressure at $\theta_{CFD} = 0$ has been chosen as the reference and set to 0.

Along with the CFD results, 4 BF solutions were considered: one without PR grooves ($C_a = C_r = 0$), and three with PR grooves, respectively for $\xi_1 = 2,10$ or 20. Fig. 6 highlights the importance of considering PR grooves in SFD simulations: the BF solutions with PR grooves are significantly closer to the CFD results. The BF solutions for the different ξ_1 are superposed, meaning that the loss have a coefficient

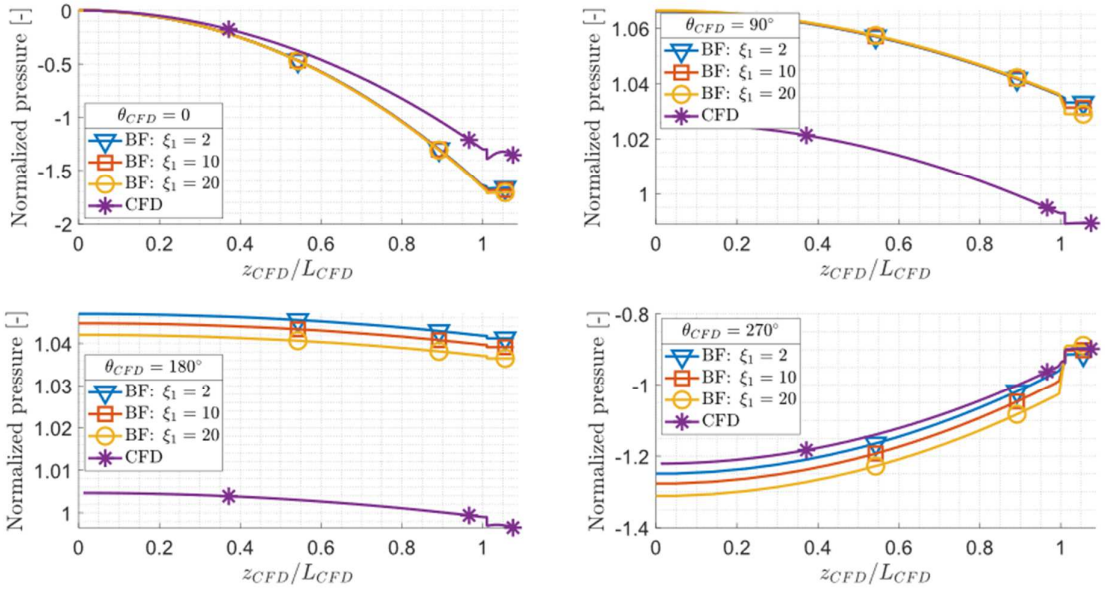

Fig. 7. Normalized pressure axial variation, $Re^* = 1$.

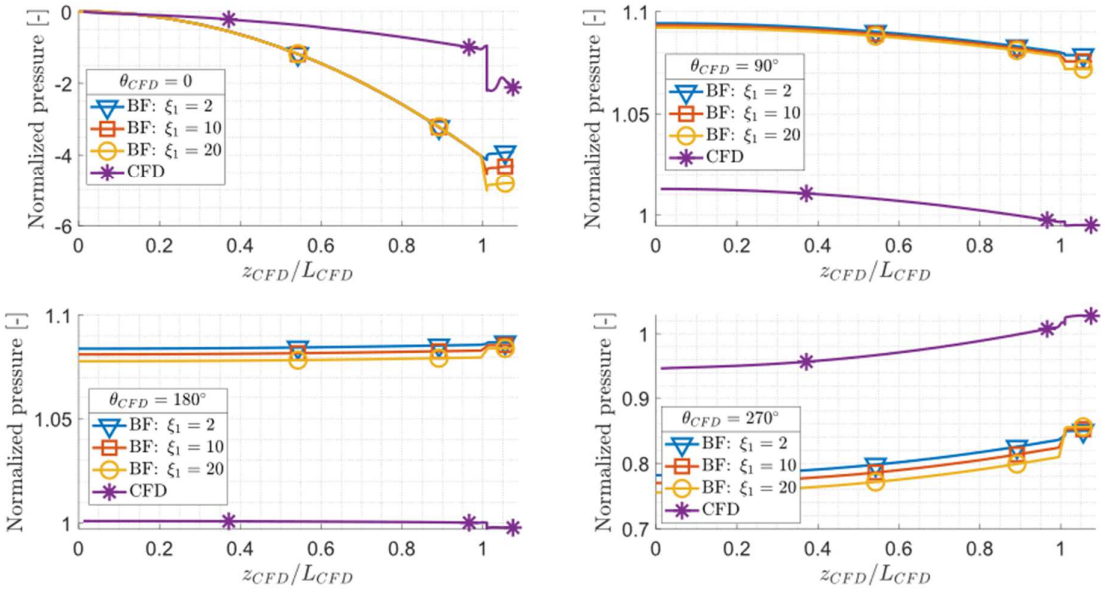

Fig. 8. Normalized pressure axial variation, $Re^* = 5$.

negligible impact of the circumferential pressure variation at the axial mid-length plane.

Fig. 7 and Fig. 8 show the pressure axial variation at different angular positions $\theta_{CFD} = \{0, 90°, 180°, 270°\}$, for $Re^* = 1$ and $Re^* = 5$ respectively. The pressure results were normalized considering the average CFD pressure at the angular position considered in each figure. The results far from the transition regions weakly depend on the value chosen for ξ_1, meaning that this parameter has a local effect, mostly impacting the solution only close to the transition regions and inside the PR clearances. Depending on the angular position considered, the best results in terms of similarity between BF and CFD solutions are obtained either for the smallest ξ_1 or for the largest one

considered. The results for $\xi_1 = 10$ are always between the ones obtained for the other values of ξ_1. Therefore, $\xi_1 = 10$ was chosen as the optimal value for describing the pressure drop at the transition region between the active length of the SFD and the axial PR clearance.

4. CONCLUSIONS

Although computationally expensive, CFD qualifies as a powerful way to refine and adjust simpler models. CFD results obtained for a simplified geometry were used to tune a BF model for SFD with PR clearances. The pressure variations occurring at the transition regions (between the SFD land and the axial PR clearance, and between the two PR clearances) were characterized by comparing CFD and BF results. A non-negligible pressure drop has been observed when the fluid enters the axial PR clearance. On the contrary, due to the lower velocities, the passage between the axial and radial PR clearances can be modeled by imposing the constancy of pressure between the two sides of the transition region.

5. REFERENCES

[1] Pietra, L. D., and Adiletta, G., 2002, *The Squeeze Film Damper over Four Decades of Investigations. Part I: Characteristics and Operating Features*, The Shock and Vibration Digest.

[2] San Andrés, L., and Delgado, A., 2007, *Identification of Force Coefficients in a Squeeze Film Damper With a Mechanical End Seal—Centered Circular Orbit Tests*, Journal of Tribology, 129(3), pp. 660–668.

[3] Lee, G. J., Kim, J., and Steen, T., 2017, *Application of Computational Fluid Dynamics Simulation to Squeeze Film Damper Analysis*, Journal of Engineering for Gas Turbines and Power, 139(102501).

[4] Patankar, S., 2018, *Numerical Heat Transfer and Fluid Flow*, Taylor & Francis.

[5] Gehannin, J., 2009, *Analyse Théorique Des Amortisseurs à Film Fluide Fonctionnant à Des Nombres de Reynolds Élevés*, Thèse de doctorat, Poitiers.

[6] Gehannin, J., Arghir, M., and Bonneau, O., 2009, *Complete Squeeze-Film Damper Analysis Based on the "Bulk Flow" Equations*, Tribology Transactions, 53(1), pp. 84–96.

ESTIMATION PAR CFD DES COEFFICIENTS DE PERTE DE CHARGE POUR LES AMORTISSEURS À FILM MINCE AVEC RAINURES D'EXTREMITE

Les amortisseurs à film mince (SFD) sont utilisés dans les moteurs aéronautiques pour ajouter de l'amortissement aux rotors flexibles guidés par des roulements à billes ou à rouleaux. L'analyse théorique des SFD est confrontée à des défis en raison du fonctionnement à haute vitesse et de la géométrie des rainures présentes dans les SFD, qui contredit l'hypothèse de film mince sur laquelle est basée la théorie de la lubrification. L'équation de Reynolds ne donne des prédictions acceptables que pour des SFDs simples à basse vitesse, ce qui est insuffisant pour les analyses dynamiques modernes des moteurs d'avion. La CFD offre des solutions précises mais couteuses du point de vue computationnel. Les équations du bulk-flow (BF), constituent une alternative moins couteuse, capable de gérer des régimes dominés par l'inertie convective (prohibitives avec une approche de type Reynolds). Les rainures d'alimentation et les rainures des segments d'étanchéités sont prises en compte dans le modèle BF en utilisant des coefficients de perte de pression ou de récupération locaux. Par conséquent, l'approche BF repose sur la détermination de ces coefficients externes, difficiles à prédire expérimentalement. La CFD est alors une alternative viable pour estimer ces coefficients. Dans le présent travail, nous montrons comment les informations locales sur les pressions et les vitesses obtenues à partir de la CFD peuvent être utilisées pour améliorer les modèles BF.

Emanuele GIAMPAOLO, Eng., Safran Aircraft Engines, emanuele.giampaolo@univ-poitiers.fr,
Mihai ARGHIR, Professor, University of Poitiers, mihai.arghir@univ-poitiers.fr,
Hugo FESTJENS, Eng., PhD, Safran Aircraft Engines, hugo.festjens@safrangroup.com.